Available online at www.sciencedirect.com
ScienceDirect
Journal of Power Sources 168 (2007) 211–217
JOURNAL OF POWER SOURCES
www.elsevier.com/locate/jpowsour

PEM stack test and analysis in a power system at operational load via ac impedance

Wenhua H. Zhu, Robert U. Payne, Bruce J. Tatarchuk *

Center for Microfibrous Materials Manufacturing, Department of Chemical Engineering, 207 Ross Hall, Auburn University, AL 36849-5127, USA

Received 1 February 2007; received in revised form 27 February 2007; accepted 28 February 2007
Available online 8 April 2007

Abstract

This paper presents a method for collecting ac impedance data from a commercial PEFC power system at operational loads. The PEM fuel cell stack in the power system, including 47 MEAs, was operated using room air and pure hydrogen (>99.99%). For a stack test in the power system, the power source for the embedded controller board was simultaneously switched from the fuel cell stack to a similar external power source after the system reached a steady temperature. The PEM fuel cells in the stack were tested by collecting the ac impedance data at different current levels. By using ac impedance, a single fuel cell, a group of fuel cells, and a complete stack were then tested without the embedded control devices for ohmic, activation, and mass transport losses. The ohmic resistance for each cell component in the stack was obtained as 117 mΩ cm^2 at operational loads from 2.5 A to 35 A. The membrane thickness was further estimated as ca. 51–89 μm. Resistances from ohmic conduction, anode/cathode activation, and mass transport were measured and discussed using the Nyquist plots from the ac impedance spectra.
© 2007 Elsevier B.V. All rights reserved.

Keywords: Fuel cell characterization; AC impedance; Stack evaluation and diagnosis; Proton exchange membrane fuel cells

1. Introduction

During the past 20 years, fuel cell related engineering sciences and technologies have attracted more attention due to the need for an efficient, non-polluting power source for global transportation (cars, buses, ships, and submarines), for portable devices (mobile communication, lap-top, and vacuum tools), and for residential backup (combined power and heat generation with top-level energy efficiency) [1,2]. Properly designed fuel cell systems can be a reliable and durable method to produce environmentally friendly energy for many applications. The polymer–electrolyte fuel cell (PEFC) is considered by many to be the most promising type of fuel cell for transportation and mobile power sources because of its low-temperature operation and ease of construction [3]. Significant progress is being made towards commercialization of producing PEFC power systems that attain the optimum balance of cost, efficiency, reliability, and durability. Characterization of a single fuel cell, a group of fuel cells, or fuel cell stacks in operation mainly refers to the electrochemical in situ techniques [4].

Electrochemical impedance spectroscopy (EIS or ac impedance) is the most powerful tool for the determination of the ohmic, activation, and concentration losses. Diard et al. [5] conducted impedance measurements (load $R = 1\ \Omega$) of a four-cell HPower stack using pure H_2 and O_2 and estimated that the resistance of the polymer membrane was ca. 40% of the internal resistance. Hakenjos et al. [6] tested their self-developed four-cell short stack using a multichannel frequency response analyzer allowing simultaneous impedance measurement of single cells (shunt resistor 100 mΩ). Yuan et al. [7] performed impedance measurement of a 500 W six-cell PEM stack using hydrogen and air. Excellent impedance arcs including air mass transport and anode activation loss demonstrated the effects of air shortage at 30 °C and 50 °C. Canut et al. [8] investigated Hydrogenic PEM stacks with 4–22 MEAs under membrane drying, fuel cell flooding, and anode catalyst poisoning conditions. For the above research and impedance work, the operating stoichiometry was maintained at 1.2–2.5, and relative humidity was controlled at 50–100%.

The drawbacks of the impedance technique are as follows: the process is complicated, the equipment is expensive,

* Corresponding author. Tel.: +1 334 844 2023; fax: +1 334 844 2063.
E-mail address: brucet@eng.auburn.edu (B.J. Tatarchuk).

0378-7753/$ – see front matter © 2007 Elsevier B.V. All rights reserved.
doi:10.1016/j.jpowsour.2007.02.071

data interpretation is difficult, and high-power application is more sophisticated. The valuable information from impedance data can be simulated by non-linear least square fitting and interpreted using equivalent circuit elements, which is called equivalent circuit modeling. The present work mostly focuses on collecting ac impedance data from a fuel cell power system directly at operational loads. Impedance data samples and theoretical analysis are conducted in order to understand the phenomenon responsible for these test results. This paper makes use of the ac impedance technique to characterize a single fuel cell, a fuel cell group, or a whole stack in a fuel cell power system.

2. Experimental details

The PEM stack in the Ballard Nexa^{TM} fuel cell system was employed in the lab test. The power module is a small, low maintenance, fully automated, and highly integrated fuel cell system providing 1200 W of unregulated dc power. Its output current can reach 44 A, and stack voltage for 47 total fuel cells normally rises up to 41 V open-circuit. Due to the inexistence of manufacturing data, the fuel cell working area is estimated as ca. 122 cm^2. The automated operation is maintained by an embedded controller board. The controller uses the stack power to adjust the parameters for optimization of energy efficiency. For the stack test in the power system, the power source for the embedded controller board can be simultaneously switched from the fuel cell stack to a similar external power source after the system reached a steady temperature. The constant voltage level for the external power source is determined easily by measuring the stack voltage delivered to the controller after the stack reaches its steady state. The PEM stack, separated from the control subsystem, was tested for collecting the ac impedance data at different current levels. The supply pressures to the stack were 5.0 psig for the fuel and 2.2 psig for air oxidant. The stack was air cooled and had no external fuel and oxidant humidification. The Gamry FC350^{TM} fuel cell monitor [9] with a proper electronic load is capable of working at a high current range for measuring the ac impedance data. The Gamry ac impedance system can be normally operated up to 50 V and 300 A within a frequency range from 10 μHz to 20 kHz. The contact and wire resistance between the power output wires and the testing fuel cells was approximately measured as $R_{wc} = 0.0218\ \Omega$ using *i–V* techniques. The sinusoidal current signal from the FC350^{TM}, working in galvanostatic or hybrid impedance mode, modulated the current from single or multiple fuel cell(s) or the PEFC stack. Simultaneously, the current information at the electric load was sent to the FC350^{TM} monitor, and the fuel cell voltage was measured by the FC350^{TM} directly. The FC350^{TM} collected these data and generated the impedance data for further analysis.

The Gamry framework software allows measurements to be performed in a galvanostatic manner and a hybrid mode. Traditional measurements are performed using constant RMS amplitude for the ac signal. The problem with this technique is that the impedance of the cell varies significantly from high to low frequencies. For impedance to be accurate, the perturbation signal has to be sufficiently small to maintain a pseudo-linear *i–V* operation. Hybrid measurements compensate for the change in cell impedance as frequency is varied by changing the ac current amplitude to keep measured ac voltage at a set of value. The previously measured impedance point is used in determining the new current amplitude as the scan proceeds from 10 kHz to 10 mHz. In this work, the galvanostatic and hybrid EIS mode were applied for the experiments in order to observe the EIS behavior at various frequencies. For the entire stack in the system, it was tested with and without the embedded controller. For the impedance spectrum, the non-linear least squares fitting algorithm was applied to find the model parameters with best agreement between the model impedance spectra and the measured spectra. Future publications will present the equivalent circuit model and simulation conducted with PSpice..

3. Results and discussion

Impedance denotes an opposition to the flow of electrons or current. It can be expressed as a complex number including the real component (Z_{re}, resistance) and the imaginary component (Z_{im}, capacitance and inductance). The measured impedance data (*f*-frequency, Z_{re}, and Z_{im}) are then forwarded to data analysis, result simulation, and physical interpretation. Because the Nyquist plot is one of the popular formats for evaluating electrochemical impedance data, a schematic drawing of a Nyquist plot is given as Fig. 1 according to both the published work [4,10] and the experimental results. This schematic description allows better understanding of the in situ impedance data on the Nyquist plots.

3.1. Small signal applied to the EIS test

Gamry indicates that a small ac signal (1–10 mV) is generally applied to a cell in a normal EIS test [11]. EIS techniques normally use very small excitation amplitudes, often in the ranges of 5–10 mV peak-to-peak [12]. The small excitation signal causes only minimal perturbation of the electrochemical test system, which ensures a pseudo-linear *iR* relationship. There is no large non-linear response to the dc potential in the cell test, because the current is measured only at the excitation frequency. This small signal reduces errors caused by measuring over a non-linear por-

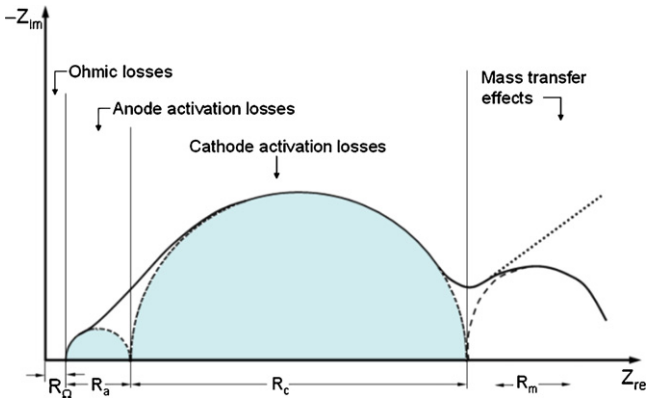

Fig. 1. Nyquist plot from a hypothetical PEM fuel cell stack (or fuel cells in the stack). The four regions represent four losses in the fuel cells, and the size of each loop is correlated to the relative magnitude of each losses.

tion of the *iR* curve. For each test, the fuel cell system was started at a constant power or current level until it reached a steady temperature. Using the hybrid EIS mode, different small ac voltages from 5 mV to 300 mV were entered into the window interface as "AC Voltage". Results reveal that the ac potential of 5 mV is so small that the points of the impedance data are scattered especially at the low frequency region. This means that 5 mV excitation signal is not strong enough to cause the useful perturbation in the electrochemical system. The rest of the data points for the ac potential signals from 20 mV to 300 mV are approximately located on the same Nyquist curve. The impedance test was also conducted using ac current as the control variable from 20 mA to 500 mA. This is called Galvanostatic EIS mode, in which a constant ac current is applied and the resulting ac potential is measured. The Nyquist data from 20 mA ac excitation is random, while data from 60 mA to 500 mA ac signals are well matched.

The Galvanostatic EIS is the most common EIS technique for fuel cell studies, but it must be used carefully [9]. In consideration of single cell or cell groups at low temperature with higher impedance (activation losses), the hybrid EIS mode is applied to set an initial current, then the ac current is adjusted continually throughout the measurement to control the ac voltage. In this manner, the amplitude of the ac current is regulated so that the ac voltage does not extend beyond the linear range.

3.2. Ohmic resistance in the Nyquist plots

The resistance R_Ω (as shown in Fig. 1) represents the total ohmic resistance of the fuel cell(s). It can be expressed as a sum of the contributions from the uncompensated wire/contact resistance R_{wc} and ohmic resistances of each cell component, R_s. Resistance of a single cell component consists of the ohmic resistance of the membrane R_m, anode R_a, cathode R_c, bipolar plates R_{bp}, and the contacts between the electrode/membrane and electrode/bipolar plate. The resistance for proton transport (ionic resistance) exists in the membrane electrolyte and also in the catalyst layer containing small amounts of Nafion additive. The opposition to electron conduction in solid materials is called electric resistance.

It is quite difficult to determine the exact contribution of the different components. For fuel cell stacks, R_m is the main contributor because the electric resistance of bipolar plates and contact layers/slots can be minimized through using highly conductive materials. The membrane resistance is inversely proportional to the surface area of the fuel cell working area. Many works focus on improving the proton conductivity of the membrane [1]; however, for impedance tests on a single cell or a three-cell group of the stack, the total ohmic resistance changes with the humidity of the membrane at room temperature operation (Fig. 2). Because the contact area is the same during tests, it is assumed that the contact resistance is the same for each test. The membrane resistance correlates to the condition of the humidity exchanger. For the whole stack, the total ohmic resistance [10] is a function of the cell number (n)

$$R_\Omega = R_{wc} + nR_s \quad (1)$$

Using this equation, it is possible to approximately predict the ohmic resistance of each cell component.

3.3. Single cell tests and impedance data interpretation

The fuel cells in the stack (#308) were tested separately at currents of 0.2 A, 0.5 A and 1.0 A dc. After the stack was started, the embedded controller was separated from the system by applying a similar current using an external power supply. The ohmic resistance is located on the Z_{re}-axis at the high frequency side of the impedance spectrum (Fig. 2). The fuel cells in the stack are fed counter-currently with air and hydrogen. They are numbered from the hydrogen inlet side to the hydrogen exhaust side. Cells #10, #15, and #25 are located near the hydrogen inlet side, far away from the humidity exchanger at the cathode inlet. The main difference among five individual fuel cells is the impedance behavior of the 47th cell in the stack. The 47th cell is located nearest to the humidified air inlet after the humidity exchanger and has the lowest ohmic resistance (R_Ω = 0.12 Ω). The mass transport losses are observed at the 47th cell due to impurity build-up. As shown in Fig. 2, there is no obvious difference in ohmic (membrane) resistance if the test current changes for the same cell. Cells #10, #15, and #25 at the front side of the stack have a slightly higher resistance (R_Ω = 0.30–0.48 Ω) at a current from 0.2 A to 1.0 A because of the less humid environment. For the single-separated fuel cell test in a stack, a small humidity gradient accounts for the disparity in ohmic resistance between cells nearby and far from the humidity exchanger.

3.4. Group cell tests and impedance data interpretation

The results for the fuel cell groups of 12, 24, 36, and 47 cells are shown in Fig. 3. The activation loss (i.e. the polarization resistance) is exceedingly higher, because a temperature of 26 °C is relatively low for the operation of PEM fuel cells. The polarization resistance (R_p) is the sum of the anode activation losses (R_a) and the cathode activation losses (R_c). It increases with the number of fuel cells in the group, and approximately

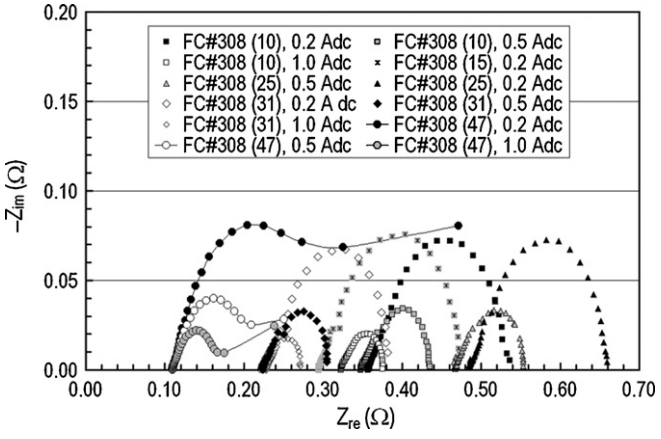

Fig. 2. Nyquist plot of stack #308 using 10–20 mV ac voltage signals entered into the hybrid EIS mode without an embedded system controller at a test-starting current from 0.2 A to 1.0 A and a temperature of ca. 26 °C.

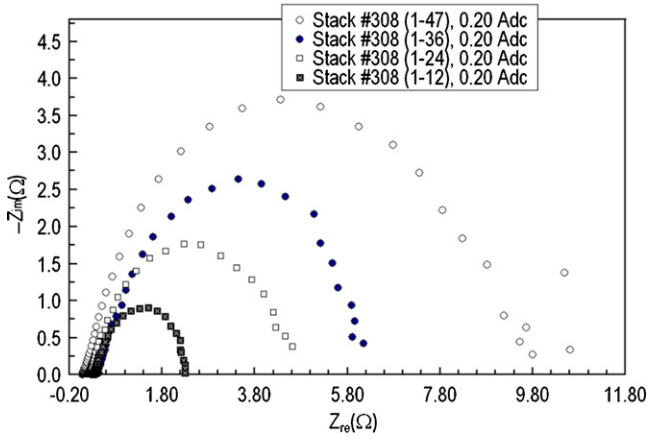

Fig. 3. Nyquist plot of stack #308 using 10 mV ac voltage signals entered into the hybrid EIS mode without an embedded system controller at a test-starting current of 0.20 A dc current and a temperature of 26 °C.

equals the sum of each cell's polarization resistance ($R_{p,i}$).

$$R_p = \sum_{i=1}^{n} R_{p,i} \approx n R_{p,1} \quad (2)$$

Four different cell groups were tested at 0.2 A load current and 26 °C. The cells were grouped in multiples of 12 up to the maximum number of cells (47). The effect of the cell numbers on the total ohmic resistance can be neglected because most of the impedances are contributed by the electrode polarization at a temperature of 26 °C. The polarization loop data can be extrapolated to the Z_{re}-axis in order to estimate the polarization resistance. The 12-group cell resistance ($R_p = 2.1\ \Omega$) is almost doubled ($R_p = 4.3\ \Omega$) if it is extended to a 24-group cell, and tripled ($R_p = 6.3\ \Omega$) if it is extended to a 36-group cell. The resistance of the last 47-group cell (stack) is 8.9 Ω. From the Nyquist plot and data analysis, it is clear that the polarization resistance for the electrode activation losses is dominant in the fuel cell reactions for low-temperature PEFC operation.

The stack was then loaded with 5 A current maintaining a temperature of 29 °C (Fig. 4). Because mass transport limitations occur at the low frequency side, impedance data are scattered on the Nyquist plot in said region. If the data points at the end loop of activation loss are extrapolated to the Z_{re}-axis, the polarization resistance approximately follows the relationship of Eq. (2). After the peaks of the imaginary impedance component, especially at the low frequency side, the loop data digress away from the normal loop curves. This is because mass transport limitations are occurring inside the fuel cells. At a 5 A load current, the mass transfer losses change the normal loop shape and size. The effects of mass transport become visible on the loop curves, especially for the total 47 fuel cells. This is identical with the anode purge cell pair located near to the 47th cell. In comparison of the ac current perturbation work [7], the Nyquist data points collected by the hybrid EIS mode appear to be a hydrogen mass transport limitation occurrings in the purge-cell pair.

3.5. Stack test and impedance data interpretation

The stack #308 was tested with its embedded controller using 500 mA ac perturbation signal. This perturbation signal has a better Nyquist plot, as shown in Fig. 5. Because of the embedded control operation, the Nyquist plot has some fluctuation or noise. The difference between this plot using 500 mA ac signal and the previous Nyquist plot appears at the low frequency end. The changes are mostly caused by mass transport loss at the air cathode side. The steady temperature for the stack is ca. 32 °C at an output current of 5 A. There are four types of losses on the single Nyquist curve as shown in Fig. 1. Ciureanu and Roberge [10] performed related work on the impedance spectrum and presented several interesting Nyquist plots about the air cathode. From the above mentioned tests and analysis for the frequency loop, it is concluded that the cathode activation losses and cathode mass transfer losses exist at the low frequency side of the Nyquist plot, and the loop size related to mass transport increases with the current in the stack.

The bigger loop, at a current of 5.0 A, is the loss due to anode and cathode activation. At the same time for the fuel cell stack, the small loop at the low frequency side is mostly related to

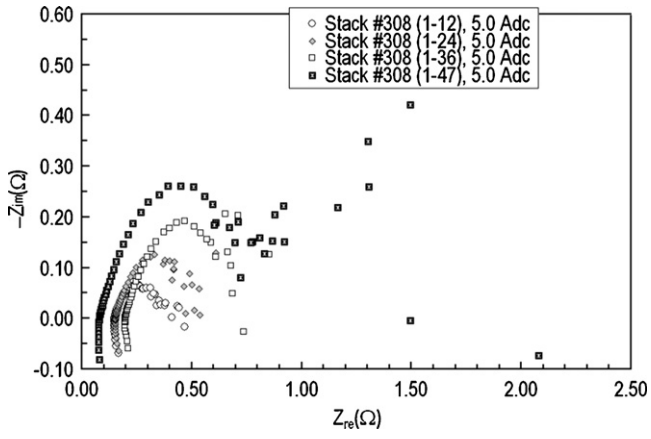

Fig. 4. Nyquist plot of stack #308 using 10–20 mV ac voltage signals entered into the hybrid EIS mode without an embedded system controller at a test-starting current of 5.0 A dc current and a temperature of 29 °C.

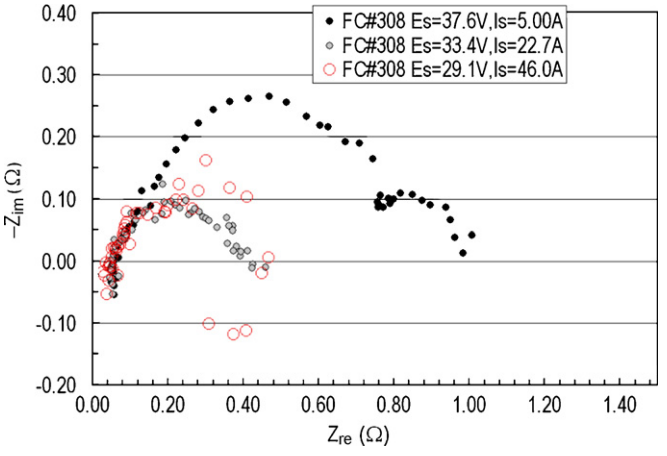

Fig. 5. Nyquist plot of stack #308 using 500 mA ac current signals applied to the PEFC stack with an embedded system controller at a test-starting current from 5.0 A, 22.7 A to 46 A and a temperature of 33 °C, 54 °C, 65 °C.

the mass transfer losses occurring at the cathode side. The loop shape is different from the hypothetical fuel cell in the literature [4], which uses an equivalent circuit model simulating mass transport loss through an infinite Warburg element at the cathode. The small loop on the low frequency side for the whole stack is similar to the Nyquist plot of the air cathode at a certain air flow rate. The difference in the loop portion associated with mass transport loss can be attributed to the different design of the fuel cell systems. Mass transport at the anodes or the cathodes may be alternatively dominant at different operating conditions due to the design of various controls or a change in operating parameters such as stoichiometry values and purge frequencies. By increasing the power output level, the activation loop is reduced and the mass transfer loss is increased. At a stack current of 46 A, the controller and mass transport limitations scatter the Nyquist data points. The exhaust of the air cathode, including, N_2, product of water, and other impurities, needs to be removed in order to allow the oxygen reactant to diffuse into the absorption/reaction sites. At a 1339 W high-power level (stack current equals to 46 A), the mass transport losses increase for cathode processes at the low frequency (right) side of the loop, as shown in the Nyquist plot (Fig. 5). It is concluded that the controller adjustment causes the data point fluctuations in comparison with the Nyquist diagram without embedded controls (Fig. 6). On the other hand, as stack temperature increases, the activation loss is largely reduced.

A recent publication [13] shows us that the reason for the departure from an ideal impedance plot (Fig. 1) is not only due to the different operating conditions experienced by the cells but also because these conditions also vary along the cell length (inlet to outlet direction). However, it is well known that the double layer capacitance is correlated to the impedance arc and is proportional to the surface area of the electro-catalysts. If the anode is loaded with enough electro-catalysts with high surface area, the impedance arc theoretically exists for anode activation loss. Since the reaction is limited more at the air cathode, the catalyst/carbon loading at the cathode is doubled in order to reduce the limitation and match with the anode feature [14]. The reduced catalyst/carbon loading could be one of the reasons for the impedance arc departure from an ideal impedance plot, because the reduced anode impedance arc is hidden in the larger cathode impedance loop.

The authors noticed that Yuan et al. [7] tested a 500 W six-cell PEM stack using hydrogen and air. The MEA in this stack consists of Nafion 115 membrane with a total Pt catalyst loading of 1.0 mg cm^{-2}. This work with higher loading of electrocatalyst shows excellent impedance arcs including anode activation loss, cathode activation loss, and air mass transport loss during air shortage operation at 30 °C and 50 °C. The impedance arc departure from an ideal impedance plot usually occurs for a whole fuel cell or stack due to optimization of the electrode structure and performance.

After the embedded controller was disabled, its power was switched simultaneously to the external power supply, and then the ac impedance data were collected for the whole stack at different current levels. The Nyquist plots are shown in Fig. 6(a and b). These Nyquist plots, after moving the noise of the

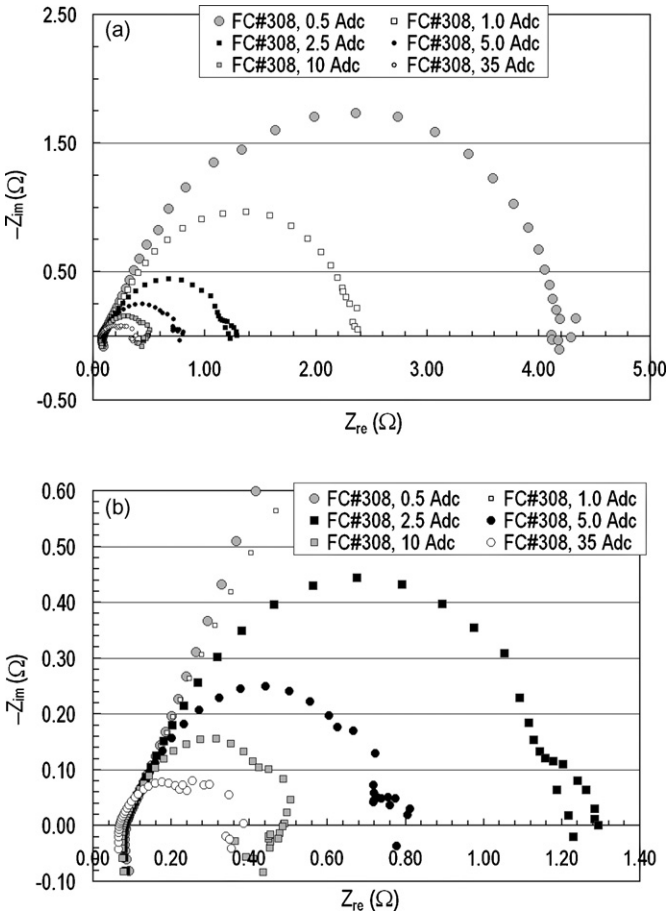

Fig. 6. Nyquist plot of stack #308 using 250–500 mA ac current signals applied to the PEFC stack without an embedded system controller at a test-starting current from 2.5 A (250 mA ac, the rest are applied with 500 mA ac current) to 35 A and a temperature from 29 °C to 65 °C. (a) Complete Nyquist diagram and (b) enlarged part of the Nyquist diagram.

embedded system controller away from the fuel cell system, describe the real reactions and processes occurring in the fuel cell stack. Mass transport losses at the low frequency side are clearly shown on these six plots. The ohmic resistance from the Nyquist plot is $R_\Omega = 0.067\ \Omega$. The resistance for each cell component R_s is calculated as $R_s = 117\ m\Omega\ cm^2$ using Eq. (1). At a current density of no more than 350 mA cm^{-2}, the saturated membrane resistances are simulated as 40–125 $m\Omega\ cm^2$ for 50–175 μm membrane [15]. The membrane thickness for the fuel cell stack is reasonably located in the range from 50 μm to 164 μm (Table 1). Based on the published *i*–*V* diagram [16], it is reasonable to assume that the membrane resistance equals half of the resistance of each cell component, so the membrane resistance is obtained as 59 $m\Omega\ cm^2$. Through linear interpolation as shown in Table 1, the membrane thickness is further estimated as ca. 82 μm, which is very close to the thickness of the Nafion® 1135 (3.5 mil, 89 μm); however, the membrane thickness was measured as 114 μm (4.5 mil) on the small edges around the stack. If the MEA in the stack uses 114 μm thick membrane, it is not acceptable that the membrane resistance approximately equals to 70% resistance of a single cell component. The reason is that the membrane may be treated on the

Table 1
Membrane thickness estimation using linear interpolation

Membrane resistance ($m\Omega\,cm^2$)	Membrane thickness (μm)		Relationship between membrane resistance (R_m) and each cell component (R_s)	Membrane data reference $R = L/\sigma$ (L: thickness (μm); σ[b]: conductivity, 0.083 $S\,cm^{-1}$)
	Simulated resistance vs. thickness[a] [15]	Estimated values by interpolation		
40	50		$R_m = 0.34R_s$	Nafion® 112 (51 μm, 61 $m\Omega\,cm^2$)
41		51	$R_m = 0.35R_s$	
59		82	$R_m = 0.50R_s$	Nafion® 1135 (89 μm, 107 $m\Omega\,cm^2$)
63		89	$R_m = 0.54R_s$	
70	100		$R_m = 0.60R_s$	Nafion® 115 (127 μm, 153 $m\Omega\,cm^2$)
81		(114)[c]	$R_m = 0.70R_s$	Nafion® 117 (178 μm, 214 $m\Omega\,cm^2$)
90		127	$R_m = 0.77R_s$	
100	140		$R_m = 0.85R_s$	
117		<164	$R_m < R_s$	
125	175		–	

[a] The simulated memebrane resistance and thickness can be viewed as constant at a current density of less than 350 $mA\,cm^{-2}$. The literature membrane was saturated before entering into the H_2/air PEM fuel cell.
[b] DuPont product information, Nafion® PFSA Membranes, NAE101, November 2002.
[c] The membrane thickness was measured at the small edges around the stack.

edges and become thicker for the edge sealing purpose. In considering that the minimum end-of-life (EOL) time is designed as 1500 h, the membrane thickness is estimated in the range between 51 μm and 89 μm. Diard et al. [5] utilized the constant membrane thickness (estimated as Nafion® 1135) and membrane conductivity ($\sigma = 0.083\,S\,cm^{-1}$) to calculate the polymer membrane resistance as ~40% of the internal resistance. This is a good theoretical value, but it neglects the thickness change during membrane compression and MEA formation. In consideration of membrane compression during hot press, the ratio of the membrane resistance to the total internal resistance is reasonably less than 40%, so the membrane resistance is close to Nafion® 112 (Table 1). Its theoretical membrane resistance is 61 $m\Omega\,cm^2$ at a thickness of 51 μm. The actual thickness in the MEA structure is estimated as ca. 34 μm based on the 33% compression ratio (i.e. the ratio of simulated membrane resistance to its theoretical membrane resistance).

In comparison with the schematic drawing (Fig. 1), mass transport at the cathode affects the reactions at a current of 2.5 A and greater (Fig. 6b). The loop portion for mass transport limitation increases with the output current levels. At the 35 A output current, the loop portion of mass transport dominates almost half of the whole Nyquist plot. It reveals that the cathode activation losses are quickly reduced as temperature increases, but mass transport limitations inside the micropores and at the active sites increase with the power output level due to the mass transfer requirement for further reactions. Removal of the gas-phase exhaust (mostly nitrogen diffusion) and transport of water product (through heat transfer and pressure driving-force) are necessary for allowing fresh reactants to diffuse into the electrode reaction zone and continuously generate the electric power.

4. Conclusion

The EIS technique is an important tool to characterize a fuel cell stack or its system. For an individual fuel cell tested separately in a power system with a humidity exchanger, its ohmic resistance(R_Ω) changes slightly with the cell location due to the humidity limitation., The ohmic resistance for each cell component in the stack is approximately obtained as 117 $m\Omega\,cm^2$ at current from 2.5 A to 35 A. When the stack is electrically isolated from the embedded controller, the Nyquist plots are less noisy; hence, the reactions and processes are better described. The mass transport loss at the anode is observed from single cell and group cell tests and the loss is caused by the impurity build-up at the purge-cell pair. The pure stack Nyquist plot shows that mass transport losses at the cathode side approximately equal the activation losses at a 35 A stack output current (ca. 287 $mA\,cm^{-2}$). The mass transport loss is observed from the stack impedance test and the loss is contributed by cathode air shortage. The mass transport losses are increased with increasing stack power output, while the activation losses are greatly reduced with increasing stack temperature. The membrane thickness is estimated in the range between 51 μm and 89 μm; its actual membrane resistance approximately equals to 35–54% of its total internal resistance. These ac impedance data can be further utilized to develop the equivalent circuit model for simulating the in situ stack behavior using the PSpice tool. The ac impedance method is simple and trouble-free for implementing real time diagnostic capability suitable for evaluating the stack performance and the state-of-health of the fuel cells in the PEM stack.

References

[1] S. Gottesfeld, T.A. Zawodiznski, in: R.C. Alkire, H. Gerischer, D.M. Kolb, C.W. Tobias (Eds.), Advances in Electrochemical Science and Engineering, vol. 5, John Wiley and Sons, Inc., New York, 1997, p. 195.
[2] N. Wagner, in: E. Barsoukov, J.R. Macdonald (Eds.), Impedance Spectroscopy-Theory, Experiment, and Applications, second ed., John Wiley & Sons, Inc., Hoboken, New Jersey, 2005, p. 496.
[3] R.A. Lemons, J. Power Sources 29 (1990) 251.

[4] R. O'Hayre, S.-W. Cha, W. Colella, F.B. Prinz, Fuel Cell Fundamentals, 203, John Wiley and Sons, Inc., New Jersey, 2005, p. 212.
[5] J.P. Diard, N. Glandut, B.L. Gorrec, C. Montella, J. Electrochem. Soc. 151 (2004) A2193–A2197.
[6] A. Hakenjos, M. Zobel, J. Clausnitzer, C. Hebling, J. Power Sources 154 (2006) 360–363.
[7] X. Yuan, J.C. Sun, M. Blanco, H. Wang, J. Zhang, D.P. Wilkinson, J. Power Sources 161 (2006) 920–928.
[8] J.M.L. Canut, R.M. Abouatallah, D.A. Harrington, J. Electrochem. Soc. 153 (2006) A857–A864.
[9] Gamry Instruments, FC350™ Fuel Cell Monitor, Warminster, PA, 2002, pp. 1–4.
[10] M. Ciureanu, R. Roberge, J. Phys. Chem. B 105 (2001) 3531–3539.
[11] Gamry Instruments, Electrochemcial Impedance Spectroscopy Primer, Warminster, PA, 2005, p. 6.
[12] Princeton Applied Research, Basics of Electrochemical Impedance Specstroscopy, Application Note AC-1, 2005.
[13] I.A. Schneider, S.A. Freunberger, D. Kramer, A. Wokaun, G.G. Scherer, J. Electrochem. Soc. 154 (2007) B383–B388.
[14] S. Costamagna, Srinivasan, J. Power Sources 102 (2001) 242–252.
[15] T.E. Springer, T.A. Zawodzinski, S. Gottesfeld, J. Electrochem. Soc. 138 (1991) 2334.
[16] D.M. Bernardi, M.W. Verbrugge, J. Electrochem. Soc. 139 (1992) 2477.